Modeling and numerical simulation of action potential patterns in human atrial tissues

Luca Gerardo-Giorda

Modeling and numerical simulation of action potential patterns in human atrial tissues

Luca Gerardo-Giorda
Dipartimento di Matematica, Università di Trento - Italy

February 22, 2007

Abstract

Electrophysiology of the heart is the subject of a vast interdisciplinary literature, from medical sciences through bio-engineering, physiology, chemistry and physics. The difficulty in having access to direct measures on real patients entailed the coupling of such studies with numerical simulations. Several works have been done on this topic, focusing mainly on the behavior of the ventricles. In this paper we focus on atrial simulation: we present a reaction-diffusion model coupled with the simple Fitz-Hugh-Nagumo (FHN) model and the more complex Courtemanche-Ramirez-Nattel (CRN) model, wich has been derived explicitely for human atrial cells. Numerical experiments are performed with both the bidomain and the monodomain models to simulate the evolution of a complete heartbeat.

1 Introduction

The basic property of neural cells to produce signals is called Action Potential (AP). It consists of a sudden variation in the transmembrane potential, called upstroke, followed by a recovering of the resting condition. It shows different shapes and amplitudes according to the different kind of excitable media to which the cells belong to, and in the large muscle cells makes it possible the simultaneous contraction of the whole cell. An action potential propagates keeping the same shape and amplitude all along an entire neural or muscular fiber. Cardiac cells are characterized by a transmembrane potential that is negative at rest, owing to the fact that the concentration of potassium ions $[K^+]_i$ inside the cardiac cell is remarkably higher than the outside concentration $[K^+]_e$, and show two kinds of action potentials: the quick and the slow response.
The quick response is typical in the myocardium fibers (both atrial and ventricular) and in the Purkinje fibers, which are fibers specialized in the conduction. The quick response cells are characterized by a negative transmembrane potential at rest (around -90mV), and by a rapid depolarization (positive overshoot), where the potential difference changes sign and the internal potential overtakes the external one of around 20mV: such phase is called Phase 0. Immediately after that (Phase 1) a short period of partial repolarization takes place, followed by a plateau (Phase 2) which lasts for around 0.2 seconds. The potential gets progressively more negative (Phase 3) until it reachs again the resting value. The repolarization procedure is far slower than the depolarization one, and the interval between the end of the repolarization and the next action potential is called Phase 4.
The slow response is the one taking place in the Sinoatrial Nodus (SA), the natural pacemaker of the heart, and in the Atrioventricular Nodus (AV), the tissue meant to transfer the pulse from atria to ventricles. The slow response cells are charcterized by a resting potential less negative (around -50mV), and by a smaller slope and amplitude in the overshoot of the action potential, the absence of the Phase 1, and by a relative refractory period that continues during Phase 4.
The Action Potential propagates across the heart in an heterogeneous way. The pulse moves from the Sinoatrial Nodus (SA), and propagates through the ordinary myocardic fibers of the right atrium, while the Buchmann's bundle drives the pulse towards the left atrium. Some action potentials propagate downwards and reach the Atrioventricular Nodus (AV), which is, under normal conditions, the only gate for the pulse

to propagate from atria to ventricles. Moreover, the conduction is slower in atria than in ventricles (1 ms^{-1} versus 4 ms^{-1}).
The electrical activity of the heart as a whole is thus characterized by a complex multiscale structure, ranging from the microscopic activity of ion channels in the cellular membrane to the macroscopic properties of the anisotropic propagation of the excitation and recovery fronts in the whole heart. The most complete model of such a complex setting is the anisotropic Bidomain model (see [9, 23]), that consists of a system of two degenerate parabolic reaction-diffusion equations describing the intra and extracellular potentials in the cardiac muscle, coupled with a system of ordinary differential equations describing the ionic currents flowing through the cellular membrane, that are associated to the nonlinear reaction term. This model is computationally very expensive because of the involvement of different space and time scales, and a simplified tissue model is the anisotropic Monodomain system, consisting of a parabolic reaction-diffusion equation describing the propagation of the transmembrane potential coupled with an ionic model, which has been widely used in literature (see for instance [21, 17]).
If, on the one hand, a wide literature is available for ventricular models (see for instance [4, 5, 18] and references therein), on the other hand less has been done on atria, althought Atrial Fibrillation (AF) is the most commonly sustained arrythmia, for which clinical treatment remains the most problematic. Knowledge of the human atrial Action Potential and of its ionic currents is thus of critical importance to understand the electrical properties of atrial tissues in both normal and pathological conditions.
In this paper we describe the Fitz-Hugh-Nagumo (FHN) cell model in the Rogers-McCulloch variant, which is well suited to capture the excitation wavefront, but behaves very poorly in the description of the plateau phase, and the Courtemanche-Ramirez-Nattel (CRN) model, that is especially designed for human atrial cells. These models are then coupled with both monodomain and bidomain simulations on a two dimensional slab with anisotropic conduction.
The rest of the paper is organised as follows. In Section 2 we give a brief review of the mathematical models, the anisotropic bidomain and monodomain ones. In Section 3 we describe the ionic currents and the modified FHN and the CRN membrane models. In Section 4 we give the variational formulation of the problem and its finite element approximation. Finally, in Section 5, some numerical simulations on a two dimensional cartesian slab are presented, varying both the cardiac tisssue model (monodomain and bidomain) and the ionic model (FHN and CRN).

2 Description of the model

The conductivity of the cardiac cells depends upon their orientation, and in the most general case the conductivity tensor is anisotropic. The structure of the cardiac cells can be modeled, following Le Grice *et al.* ([13]) as a sequence of muscular layers going from endocardium to epicardium (see also [26]). In any point $\mathbf{x}$ it is thus possible to identify an orthonormal triplet of directions, $\mathbf{a}_l(\mathbf{x})$, $\mathbf{a}_t(\mathbf{x})$, $\mathbf{a}_n(\mathbf{x})$, with $\mathbf{a}_l(\mathbf{x})$ parallel to the fibers direction, $\mathbf{a}_t(\mathbf{x})$ e $\mathbf{a}_n(\mathbf{x})$ tangent and orthogonal repectively to the radial lamination, both transversal with respect to the fiber axis.

2.1 The bidomain model

The bidomain model consists in representing the cardiac tissue as the superposition of two media which are continuous and anisotropic, the intra-cellular and the extra-cellular one, coexisting at each point $\mathbf{x}$ and separated by a cell membrane. Such model has been derived, by an homogenization technique, starting from a periodic assembling of elongated cells surrounded by extracellular space and connected by end-to-end or side-to-side junctions (for the mathematical details we refer to [12, 6]).
Denoting by $\sigma_l^{i,e}$, $\sigma_t^{i,e}$, and $\sigma_n^{i,e}$ the conductivity coefficients in the $\mathbf{a}_l$, $\mathbf{a}_t$ and $\mathbf{a}_n$ directions, the conductivity tensor is given by

$$D_{i,e}(\mathbf{x}) = \sigma_l^{i,e}\mathbf{a}_l(\mathbf{x})\mathbf{a}_l^T(\mathbf{x}) + \sigma_t^{i,e}\mathbf{a}_t(\mathbf{x})\mathbf{a}_t^T(\mathbf{x}) + \sigma_n^{i,e}\mathbf{a}_n(\mathbf{x})\mathbf{a}_n^T(\mathbf{x}),$$

for the intra- and extra-cellular medium respectively.
The intra-cellular and extra-cellular electric potentials, which we denote by u_i and u_e, are governed in the bidomain model by a degenerate reaction diffusion system of parabolic type, coupled with an ODE system describing the ionic gating variables w and the ionic concentration c. In the following we denote

$I_m = c_m \partial_t v + I_{ion}(v,w,c)$ the membrane current per unit volume, where $c_m = \chi C_m$, $I_{ion} = \chi i_{ion}$, χ being the membrane area per tissue volume, C_m the surface capacity and i_{ion} the membrane ionic current per unit area.
Let then I_e^{app} be an applied extra-cellular current per unit volume which satisfies the compatibility condition $\int_\Omega I_e^{app} = 0$ and let $\mathbf{j}_{i,e} = -D_{i,e}\nabla u_{i,e}$ be the intra- and extra-cellular current density: the conservation of the total current entails $\operatorname{div}\mathbf{J}_i = -I_m$ and $\operatorname{div}\mathbf{J}_e = I_m - I_e^{app}$.
The bidomain model in the variables $(u_i(\mathbf{x},t), u_e(\mathbf{x},t))$ and $v(\mathbf{x},t) = u_i(\mathbf{x},t) - u_e(\mathbf{x},t)$, for an insulated domain $\Omega \subset \mathbb{R}^3$, reads then

$$\begin{cases} c_m\partial_t v - \operatorname{div}(D_i\nabla u_i) + I_{ion}(v,w,c) = 0 & \text{in } \Omega\times(0,T) \\ -c_m\partial_t v - \operatorname{div}(D_e\nabla u_e) - I_{ion}(v,w,c) = -I_e^{app} & \text{in } \Omega\times(0,T) \\ \partial_t w - R(v,w) = 0 & \text{in } \Omega\times(0,T) \\ \partial_t c - S(v,w,c) = 0 & \text{in } \Omega\times(0,T) \\ \mathbf{n}^T D_{i,e}\nabla u_{i,e} = 0 & \text{in } \partial\Omega\times(0,T) \\ v(\mathbf{x},0) = v_0(\mathbf{x}) \qquad w(\mathbf{x},0) = w_0(\mathbf{x}) \qquad c(\mathbf{x},0) = c_0(\mathbf{x}) & \text{in } \Omega. \end{cases} \tag{2.1}$$

The above system uniquely determines v, whereas the potentials u_i and u_e are determined modulus an additive constant depending on time and linked to the reference potential. Such potential is chosen as the mean extracellular potential in the cardiac volume, by imposing a zero mean condition $\int_\Omega u_e = 0$.
System (2.1) can be rewritten in terms of extracellular and transmembrane potentials. From the second equation in (2.1) we get

$$c_m\partial_t v = -\operatorname{div}(D_e\nabla u_e) - I_{ion}(v,w,c) - I_e^{app},$$

and inserting it into the first one provides

$$-\operatorname{div}\ [D_i\nabla u_i + D_e\nabla u_e] = -I_e^{app}.$$

So far, adding and subtracting $\operatorname{div}(D_i\nabla u_e)$, we obtain the formulation in terms of v and u_e:

$$\begin{cases} -c_m\partial_t v - \operatorname{div}(D_e\nabla u_e) - I_{ion}(v,w,c) = -I_e^{app} & \text{in } \Omega\times(0,T) \\ -\operatorname{div}\ [(D_i+D_e)\nabla u_e] = \operatorname{div}(D_i\nabla v) - I_e^{app} & \text{in } \Omega\times(0,T) \end{cases} \tag{2.2}$$

2.2 The simplified monodomain model

If we assume the anisotropy ratio to be the same in the two media, intra- and extra-cellular, namely we assume $D_i = \lambda D_e$ with λ constant, the bidomain model reduces to the monodomain one. If we let

$$D = \frac{\lambda}{1+\lambda} D_i, \qquad I^{app} = \frac{\lambda}{1+\lambda} I_i^{app} + \frac{1}{1+\lambda} I_e^{app},$$

the simplified monodomain model consists of a single reaction-diffusion equation of parabolic type for the transmembrane potential v.

$$\begin{cases} c_m\partial_t\, v - \operatorname{div}(D(\mathbf{x})\nabla v) + I_{ion}(v,w,c) = I^{app} & \text{in } \Omega\times(0,T) \\ \partial_t w - R(v,w) = 0 & \text{in } \Omega\times(0,T) \\ \partial_t c - S(v,w,c) = 0 & \text{in } \Omega\times(0,T) \\ \mathbf{n}^T D\nabla v = 0 & \text{in } \partial\Omega\times(0,T) \\ v(\mathbf{x},0) = v_0(\mathbf{x}), \quad w(\mathbf{x},0) = w_0(\mathbf{x}), \quad c(\mathbf{x},0) = c_0(\mathbf{x}) & \text{in } \Omega. \end{cases} \tag{2.3}$$

3 Ionic currents and membrane models

The ionic currents appearing in both the monodomain and the bidomain model rely on the choice of the membrane model for the cell conductivity. The earliest model appeared in the work on nerve action potential by Hodgkin and Huxley ([10]), which earned them the Nobel prize in Medicine in 1963. Models of this type

have then been developed for the cardiac action potential, where the variation in time of the membrane potential v (under the assumption of an equipotential cell) is given by

$$\frac{dv}{dt} = -\frac{I_{ion} - I_{st}}{C_m}, \tag{3.1}$$

where I_{ion} and I_{st} are the total ionic current and stimulus current across the membrane, respectively, and C_m is the total membrane capacitance. In (3.1) the ionic current through the channels in the membrane depends on the transmembrane potential v and on M gating and concentration variables $w \in \mathbb{R}^M$, and reads

$$I_{ion}(v, w) = \sum_{k=1}^{N} G_k(v) \prod_{j=1}^{M} w_j^{p_{jk}} (v - v_k(w)),$$

$G_k(v)$ being the membrane conductance, v_k being the reversal potential for the k-th current and p_{jk} being integers, and where the dynamics of the gating and concentration variables is described by a system of ODE's

$$\frac{\partial w}{\partial t} = R(v, w), \qquad w(\mathbf{x}, 0) = w_0(\mathbf{x}).$$

In such models, if w_j is a gating variable, the right hand side $R_j(v, w)$ has a special structure and the corresponding ODE is given by

$$\frac{\partial w_j}{\partial t} = R_j(v, w) = R_j(v, w_j) = \alpha_j(v)(1 - w_j) - \beta_j(v) w_j, \tag{3.2}$$

with $\alpha_j(v), \beta_j(v) > 0$, $0 < w_j < 1$.

Many refinements of the original Hodgkin-Huxley model, obtained by fitting improved experimental data with more complex models, have been developed for the modeling of ventricular cells: among them, we recall the model by Beeler and Reuter (1977, with 4 ionic currents and 7 gating and concentrations variables), and the phase-I Luo-Rudy (1991, with $N = 6$ and $M = 7$). In this direction, the most recent published model of mammalian ventricular cells is the phase-II Luo-Rudy (1994, [15]), which is based on measurements from guinea pig. Simpler models of reduced complexity have also been proposed, where only 1 or 2 gating variables are considered.

If, on the one hand, several models are available to describe the behaviour of ventricular cells, less has been done focusing on atrial cells. Atria differ from ventricles under several aspects. First of all, the thickness of the wall in atria is far less significant than in ventricles, while the speed of conduction is much larger in ventricles. A different ionic current and membrane model should therefore be used when dealing with atria. In this direction, models of atrial cells based on animal data only have been published (see [8, 20, 27]): the most recent of such model is the one proposed by Lindblad *et al.* (1996, [14]), which is based on measurements from rabbit atrial cells. Although these models have provided valuable insights into the mechanisms underlying the action potential generation in animals, the significant interspecies differences with respect to human being and the amount of available human data led scientists to develop mathematical models of the action potential based on ionic current data measured directly in human atrial cells. The most recently published models in this direction are the ones proposed by Nygren *et al.* in [16] and by Courtemanche *et al.* in [7]. These two models handle the atrial cell as a capacitor connected in parallel with variable resistances and batteries representing the ionic channels and driving forces.

3.1 The FHN cell model

The most used and simplest ionic model is the Fitz-Hugh-Nagumo (FHN), consisting of 1 ionic current and 1 gating variable. Assuming the potential v to be zero at rest, the ionic current uses only one recovery variable:

$$I_{ion}(v, w) = g(v) + \beta w,$$

where $\beta > 0$, $g(v)$ is a cubic-like function and w satisfies

$$\frac{\partial w}{\partial t} = \eta v - \gamma w,$$

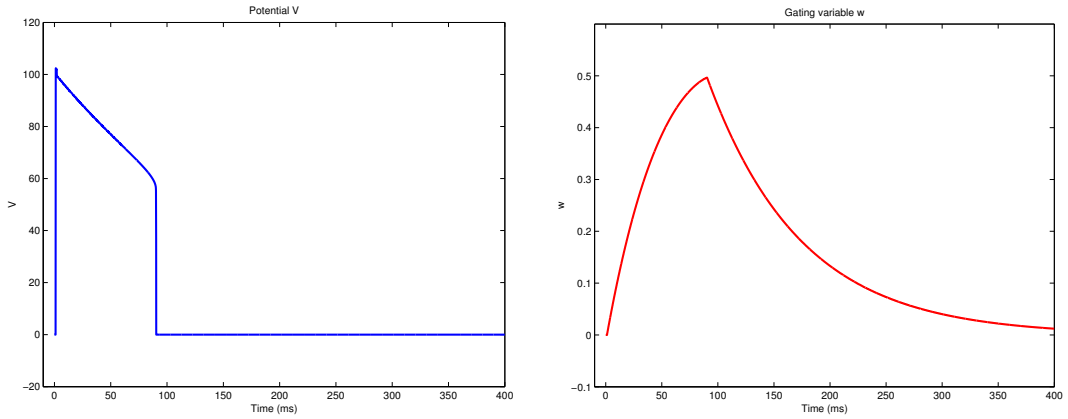

Figure 1: Time evolution of the potential v and the gating variable w in the Rogers-McCulloch variant of the FHN model

with $\eta, \gamma > 0$.
An improvement of this model is given by the following variant by Rogers and McCulloch ([21]):

$$I_{ion}(v,w) = Gv\left(1-\frac{v}{v_{\rm th}}\right)\left(1-\frac{v}{v_{\rm p}}\right)+\eta_1 vw,$$

$$\frac{\partial w}{\partial t} = \eta_2\left(\frac{v}{v_{\rm p}}-\eta_3 w\right),$$

where $G, \eta_1, \eta_2, \eta_3$ are positive coefficients, $v_{\rm th}$ is a threshold potential, and $v_{\rm p}$ is the peak potential. In Figure 1 we report the time evolution of the potential v and of the gating variable w for the Rogers-McCulloch variant of the FHN model.
If, on the one hand, such models are well suited to describe the positive overshoot in the quick depolarization phase, on the other hand they provide only a coarse approximation in the plateau and repolarization phases of the action potential, and behave too poorly when accuracy in the description of the action potential is needed.

3.2 The CRN atrial cell model

One of the most accurate models for atrial cells is the CRN (Courtemanche, Ramirez and Nattel, [7]) one, in which the total ionic current is given by the sum

$$I_{ion} = I_{\rm Na} + I_{\rm K1} + I_{\rm to} + I_{\rm Kur} + I_{\rm Kr} + I_{\rm Ks} + I_{\rm Ca,L} + I_{\rm p,Ca} + I_{\rm NaK} + I_{\rm NaCa} + I_{\rm b,Na} + I_{\rm b,Ca}. \tag{3.3}$$

In the above expression, the total ionic current take into account the fast depolarizing Na^+ current, the rectifier K^+ currents, the L-type CA^{2+} current, the background currents, the intracellular concentrations $[Ca^{2+}]_i$, $[Na^+]_i$, and $[K^+]_i$, the action of the NaK and NaCa pumps, and the handling of the intracellular calcium concentration by the sarcoplasmic reticulum system (SR). In the model, no extracellular cleft space is included, the membrane capacitance is $c_m = 100$pF, the lenght and diameter of the cells are set to 100 and 16 μm, respectively, and the cell compartment volumes are the same ones used in the phase-II Luo-Rudy model (LR2, [15]). We give hereafter a brief description of the ionic currents. In that order, we denote with E_X the equilibrium potential for ion X, and with g_X its maximal conductance. From Nerst equation, E_X is given by

$$E_X = \frac{RT}{zF}\log\frac{[X]_e}{[X]_i},$$

where R is the gas constant, T is the absolute temperature, F is the Faraday constant, $z = 1$ for Na^+ and K^+, $z = 2$ for Ca^{2+}, and $[X]_e$ and $[X]_i$ denote the external and internal concentration of ion X.

Fast Na^+ current

It is a large, rapid inward current which is the major responsible of the depolarization phase at the beginning of the action potential. It is given by

$$I_{\mathrm{Na}} = g_{\mathrm{Na}} m^3 h j (v - E_{\mathrm{Na}}),$$

where m, h, and j are gating variables, whose coefficients in equation (3.2) are given by

$$\alpha_m = \begin{cases} .32\,\dfrac{v+47.13}{1-\exp\left[-.1(v+47.13)\right]} \\ \\ 3.2, \qquad \text{if } v = -47.13 \end{cases} \qquad \beta_m = .08\exp\left(-\frac{v}{11}\right)$$

$$\alpha_h = \begin{cases} .135\,\exp\left(-\dfrac{v+80}{6.8}\right) \\ \\ 0, \qquad \text{if } v \geq -40 \end{cases} \qquad \beta_h = \begin{cases} 3.56\,\exp(.079v) + 3.1\times 10^5\exp(.35v) \\ \\ 7.69\,\left[1+\exp\left(-\dfrac{v+10.66}{11.1}\right)\right]^{-1}, \qquad \text{if } v \geq -40 \end{cases}$$

$$\alpha_j = \begin{cases} [-127,140\,\exp\left(.2444\,v\right) - 3.474\times 10^{-5}\exp(-.04391v)]\dfrac{v+37.78}{1+\exp[.311\,(v+79.23)]} \\ \\ 0, \qquad \text{if } v \geq -40 \end{cases}$$

$$\beta_j = \begin{cases} .1212\,\dfrac{\exp(-.01052v)}{1+\exp[-.1378(v+40.14)]} \\ \\ .3\,\dfrac{\exp\left[-2.535\times 10^{-7}v\right]}{1+\exp[-.1(v+32)]} \qquad \text{if } v \geq -40 \end{cases}$$

Inward rectifier K^+ current

This current plays a major role in the late repolarization phase of the AP and in determining resting membrane potential and resistance. It is given by

$$I_{\mathrm{K1}} = \frac{g_{\mathrm{K1}}(v - E_{\mathrm{K}})}{1+\exp(.07(v+80))} \qquad g_{\mathrm{K1}} = .09$$

Ultrarapid rectifier K^+ current:

$$I_{\mathrm{Kur}} = g_{\mathrm{Kur}} u_a^3 u_i (v - E_{\mathrm{K}}), \qquad g_{\mathrm{Kur}} = .005 + \frac{.05}{1+\exp\left(\frac{v-15}{-13}\right)},$$

where u_a and u_i are gating variables, which satisfy equation (3.2) with coefficients

$$\alpha_{ua} = .65\,\left[\exp\left(-\frac{v+10}{8.5}\right) + \exp\left(-\frac{v-30}{59.0}\right)\right]^{-1} \qquad \beta_{ua} = .65\,\left[2.5+\exp\left(\frac{v+82}{17}\right)\right]^{-1}$$

$$\alpha_{ui} = \left[21+\exp\left(-\frac{v-185}{28}\right)\right]^{-1} \qquad \beta_{ui} = \exp\left(\frac{v-158}{16}\right)$$

Transient outward K^+ current

$$I_{\text{to}} = g_{\text{to}} o_a^3 o_i (v - E_{\text{K}}), \qquad g_{\text{to}} = .1652,$$

where o_a and o_i are gating variables, which satisfy equation (3.2) with coefficients

$$\alpha_{oa} = .65 \left[\exp\left(-\frac{v+10}{8.5} \right) + \exp\left(-\frac{v-30}{59.} \right) \right]^{-1} \qquad \beta_{oa} = .65 \left[2.5 + \exp\left(\frac{v+82}{17.} \right) \right]^{-1}$$

$$\alpha_{oi} = \left[18.53 + \exp\left(\frac{v+113.7}{10.95} \right) \right]^{-1} \qquad \beta_{oi} = \left[18.53 + \exp\left(-\frac{v+1.26}{7.44} \right) \right]^{-1}$$

Rapid and slow delayed rectifier K^+ currents

$$I_{\text{Kr}} = \frac{g_{\text{Kr}} x_r (v - E_{\text{K}})}{1 + \exp\left(\frac{v+15}{22.4} \right)} \qquad g_{\text{Kr}} = .0294$$

$$I_{\text{Ks}} = g_{\text{Ks}} x_s^2 (v - E_{\text{K}}) \qquad g_{\text{Ks}} = .129$$

where x_r and x_s are gating variables, which satisfy equation (3.2) with coefficients

$$\alpha_{xr} = .0003 \frac{v + 14.1}{1 - \exp\left(\frac{v+14.1}{5} \right)} \qquad \beta_{xr} = 7.3898 \times 10^{-5} \frac{v - 3.3328}{\exp\left(\frac{v-3.3328}{5.1237} \right)}$$

$$\alpha_{xs} = 4 \times 10^{-5} \frac{v - 19.9}{1 - \exp\left(-\frac{v-19.9}{17} \right)} \qquad \beta_{xs} = 3.5 \times 10^{-5} \frac{v - 19.9}{\exp\left(\frac{v-19.9}{9} - 1 \right)}$$

L-type Ca^2+ current

$$I_{\text{Ca,L}} = g_{\text{Ca,L}} d f f_{\text{Ca}} (v - 65.0) \qquad g_{\text{Ca,L}} = .1238$$

where d, f and f_{Ca} are gating variables, which satisfy equation

$$\frac{dy}{dt} = -\frac{y^\infty - y}{\tau_y} \tag{3.4}$$

where y is any of d, f, f_{Ca}, with coefficients

$$\tau_d = \frac{1 - \exp\left(-\frac{v+10}{6.24} \right)}{.035\,(v+10)\,\left[1 + \exp\left(-\frac{v+10}{6.24} \right) \right]} \qquad d^\infty = \left[1 + \exp\left(-\frac{v+10}{8} \right) \right]^{-1}$$

$$\tau_f = 9 \left[.0197 \exp\left[-.0337^2 (v+10)^2 \right] + .02 \right]^{-1} \qquad f^\infty = \left[1 + \exp\left(\frac{v+28}{6.9} \right) \right]^{-1}$$

$$\tau_{f_{\text{Ca}}} = 2 \qquad f_{\text{Ca}}^\infty = \left(1 + \frac{[\text{Ca}^{2+}]_i}{.00035} \right)^{-1}$$

Ca^{2+} pump current

$$I_{\text{p,Ca}} = I_{\text{p,Ca(max)}} \frac{[\text{Ca}^{2+}]_i}{.0005 + [\text{Ca}^{2+}]_i} \qquad I_{\text{p,Ca(max)}} = .275$$

Na^+-K^+ pump current

$$I_{\text{NaK}} = I_{\text{NaK(max)}} f_{\text{NaK}} \frac{1}{1 + \left(\frac{K_{\text{m,Na(i)}}}{[\text{Na}^+]_i} \right)^{3/2}} \frac{[\text{K}^+]_o}{[\text{K}^+]_o + K_{\text{m,K(o)}}} \qquad I_{\text{NaK(max)}} = .6,$$

where $K_{\text{m,Na(i)}}$ and $K_{\text{m,K(o)}}$ are the $[\text{Na}^+]_i$ and $[\text{K}^+]_o$ half saturation constants, respectively, while

$$f_{\text{NaK}} = \left[1 + .1245 \exp\left(-.1 \frac{Fv}{RT} \right) + .0052 \left[\exp\left(\frac{[\text{Na}^+]_o}{67.3} \right) - 1 \right] \exp\left(-\frac{Fv}{RT} \right) \right]^{-1}$$

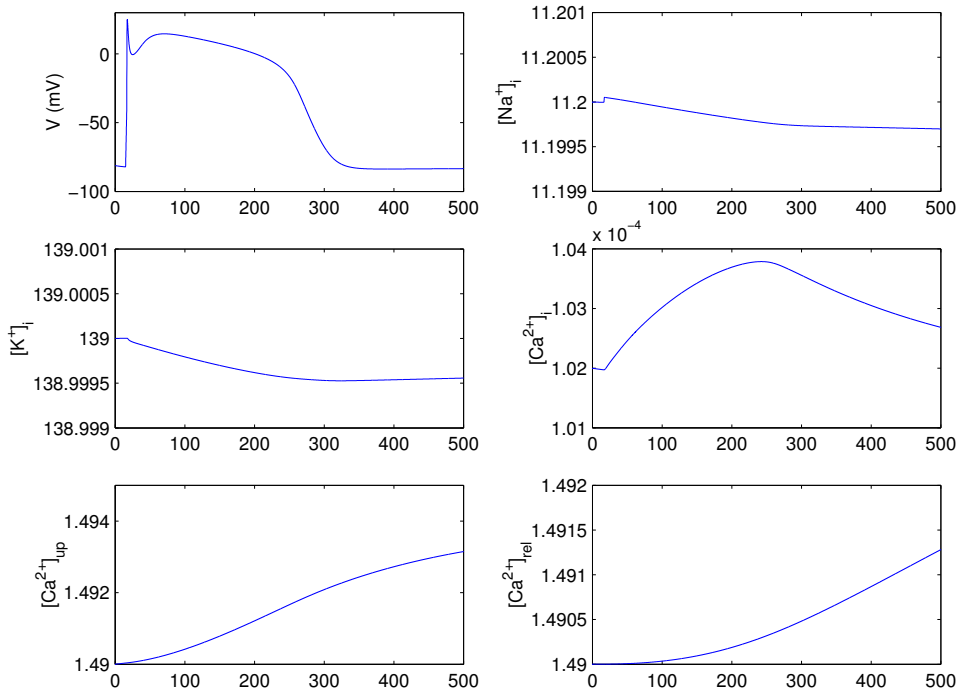

Figure 2: CRN model: potential and concentration variables.

Na^+-Ca^{2+} exchanger

$$I_{\mathrm{NaCa}} = I_{\mathrm{NaCa(max)}} \frac{\exp\left[\gamma \frac{vF}{RT}\right] [\mathrm{Na}^+]_i^3)[\mathrm{Ca}^{2+}]_o - \exp\left[(\gamma-1)\frac{vF}{RT}\right] [\mathrm{Na}^+]_o^3)[\mathrm{Ca}^{2+}]_i}{(K_{\mathrm{m,Na}}^3 + [\mathrm{Na}^+]_o^3)(K_{\mathrm{m,Ca}} + [\mathrm{Ca}^{2+}]_o)(1 + k_{sat} \exp\left[(\gamma-1)\frac{vF}{RT}\right])}$$

where $I_{\mathrm{NaCa(max)}} = 1600.0$, $K_{\mathrm{m,Na}}$ and $K_{\mathrm{m,Ca}}$ are the $[\mathrm{Na}^+]_i$ and $[\mathrm{Ca}^{2+}]_o$ half saturation constants, respectively, $k_{sat} = .1$ is a saturation factor, and $\gamma = .35$ is a voltage dependence parameter.

Background Ca^{2+} and Na^+ currents

$$I_{\mathrm{b,Ca}} = g_{\mathrm{b,Ca}}(v - E_{\mathrm{Ca}})$$
$$I_{\mathrm{b,Na}} = g_{\mathrm{b,Na}}(v - E_{\mathrm{Na}})$$

where $g_{\mathrm{b,Ca}}$ and $g_{\mathrm{b,Na}}$ are the maximal conductances for Ca^{2+} and Na^+, respectively.

Dynamics of the concentration variables and the calcium buffers

The concentration variables considered in the CRN model are the internal concentrations $[\mathrm{Na}^+]_i$, $[\mathrm{K}^+]_i$ and $[\mathrm{Ca}^{2+}]_i$, and the uptake and release calcium concentration by the sarcoplasmic reticulum, $[\mathrm{Ca}^{2+}]_{\mathrm{up}}$, $[\mathrm{Ca}^{2+}]_{\mathrm{rel}}$. Their dynamics is governed by the following equations

$$\frac{d[\mathrm{Na}^+]_i}{dt} = \frac{-3I_{\mathrm{NaK}} - 3I_{\mathrm{NaCa}} - I_{\mathrm{b,Na}} - I_{\mathrm{Na}}}{FV_i}$$

$$\frac{d[\mathrm{K}^+]_i}{dt} = \frac{2I_{\mathrm{NaK}} - I_{\mathrm{K1}} - I_{\mathrm{to}} - I_{\mathrm{Kur}} - I_{\mathrm{Kr}} - I_{\mathrm{Ks}}}{FV_i}$$

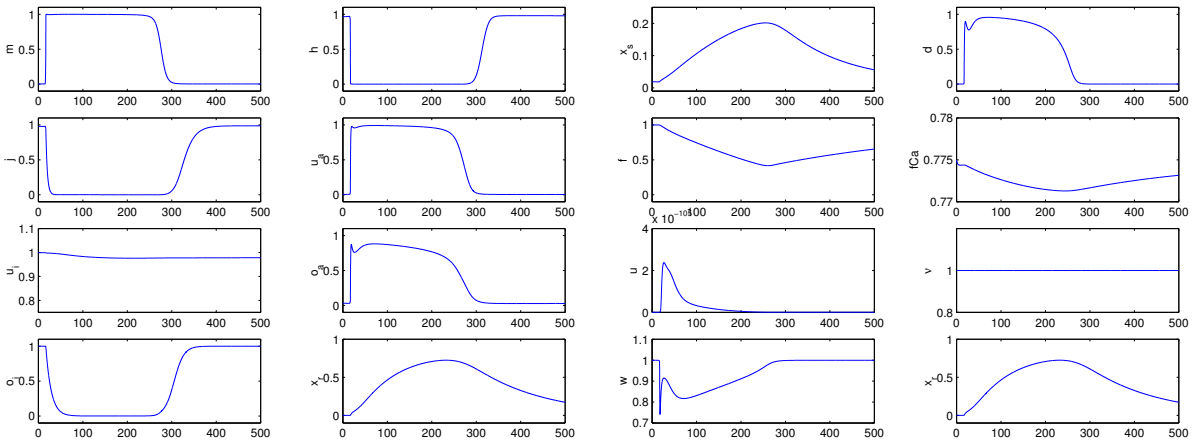

Figure 3: CRN model: gating variables.

$$\frac{d[\mathrm{Ca}^{2+}]_i}{dt} = \left[\frac{2I_{\mathrm{NaCa}} - I_{\mathrm{p,Ca}} - I_{\mathrm{Ca,L}} - I_{\mathrm{b,Ca}}}{2FV_i} + \frac{V_{\mathrm{up}}(I_{\mathrm{up,leak}} - I_{\mathrm{up}}) + I_{\mathrm{rel}}V_{\mathrm{rel}}}{V_i}\right] \times \\ \times \left[1 + \frac{[\mathrm{Trpn}]_{\max}K_{\mathrm{m,Trpn}}}{([\mathrm{Ca}^{2+}]_i + K_{\mathrm{m,Trpn}})^2} + \frac{[\mathrm{Cmdn}]_{\max}K_{\mathrm{m,Cmdn}}}{([\mathrm{Ca}^{2+}]_i + K_{\mathrm{m,Cmdn}})^2}\right]^{-1} \tag{3.5}$$

$$\frac{d[\mathrm{Ca}^{2+}]_{\mathrm{up}}}{dt} = I_{\mathrm{up}} - I_{\mathrm{up,leak}} - I_{\mathrm{tr}}\frac{V_{\mathrm{rel}}}{V_{\mathrm{up}}} \tag{3.6}$$

$$\frac{d[\mathrm{Ca}^{2+}]_{\mathrm{rel}}}{dt} = (I_{\mathrm{tr}} - I_{\mathrm{rel}})\left[1 + \frac{[\mathrm{Csqn}]_{\max}K_{\mathrm{m,Csqn}}}{([\mathrm{Ca}^{2+}]_{\mathrm{rel}} + K_{\mathrm{m,Csqn}})^2}\right]^{-1}, \tag{3.7}$$

where V_i is the intracellular volume, V_{up} and V_{rel} are the volumes of the uptake and release compartments of the sarcoplasmic reticulum (SR), $[\mathrm{Trpn}]_{\max}$ and $[\mathrm{Cmdn}]_{\max}$ are the total concentrations of troponin and calmodulin in myoplasm, $[\mathrm{Csqn}]_{\max}$ is the total concentration of calsequestrin in the release compartment of SR, while $\mathrm{K_{m,Trpn}}$, $\mathrm{K_{m,Cmdn}}$ and $\mathrm{K_{m,Csqn}}$ are their half saturation constants, respectively.
The *Ca^{2+} Leak current by the JSR* in equations (3.5) and (3.6) above is given by

$$I_{\mathrm{up,leak}} = \frac{[\mathrm{Ca}^{2+}]_{\mathrm{up}}}{[\mathrm{Ca}^{2+}]_{\mathrm{up,max}}} I_{\mathrm{up,max}},$$

where $[\mathrm{Ca}^{2+}]_{\mathrm{up,max}}$ and $I_{\mathrm{up,max}}$ are the maximal $[\mathrm{Ca}^{2+}]$ concentration in NSR and the maximal $[\mathrm{Ca}^{2+}]$ uptake rate for I_{up}, respectively.
The *Ca^{2+} Uptake current by the JSR* in equations (3.5) and (3.6) above is given by

$$I_{\mathrm{up}} = \frac{I_{\mathrm{up,max}}}{1 + (K_{\mathrm{up}}/[\mathrm{Ca}^{2+}]_i)},$$

where K_{up} is the $[\mathrm{Ca}^{2+}]_i$) half saturation constant.
The *Ca^{2+} Release current from the JSR* in equations (3.5) and (3.7) above is given by

$$I_{\mathrm{rel}} = k_{\mathrm{rel}}u^2\nu w([\mathrm{Ca}^{2+}]_{\mathrm{rel}} - [\mathrm{Ca}^{2+}]_i),$$

where u, ν and w are gating variables whose dynamics is given by equation (3.4), with coefficients

$$\tau_u = 8.0 \qquad u^\infty = \left[1 + \exp\left(-\frac{F_n - 3.4175\times10^{-13}}{13.67\times10^{-16}}\right)\right]^{-1}$$

$$\tau_\nu = 1.91{+}2.09\left[1 + \exp\left(-\frac{F_n - 3.4175\times10^{-13}}{13.67\times10^{-16}}\right)\right]^{-1} \qquad \nu^\infty = 1{-}\left[1 + \exp\left(-\frac{F_n - 6.835\times10^{-14}}{13.67\times10^{-16}}\right)\right]^{-1}$$

$$\tau_w = 6.0\frac{1-\exp\left(-\frac{v-7.9}{5}\right)}{\left[1+.3\exp\left(-\frac{v-7.9}{5}\right)\right](v-7.9)} \qquad w^\infty = 1-\left[1+\exp\left(-\frac{v-40}{17}\right)\right]^{-1},$$

where we have set

$$F_n = 10^{-12}V_{\rm rel}I_{\rm rel} - \frac{5\times 10^{-13}}{F}\left(\frac{1}{2}I_{\rm Ca,L} - \frac{1}{5}I_{\rm NaCa}\right).$$

Finally, the *Transfer current from NSR to JSR* in equations (3.6) and (3.7) above is given by

$$I_{\rm tr} = \frac{[{\rm Ca}^{2+}]_{\rm up} - [{\rm Ca}^{2+}]_{\rm rel}}{\tau_{\rm tr}},$$

where $\tau_{\rm tr} = 180$.
In Figure 2 and 3 we report the time evolution of the potential and of the gating and concentration variables.

4 Variational formulation and discretization of the model

In this section we outline a variational formulation of the monodomain and the bidomain models.
Let N be the number of gating variables, let M be the number of concentration variables of the ionic model, and let $H^1(\Omega)$ be the usual Sobolev space over $\mathbb{R}$. The variational formulation of the monodomain model reads as follows.
Given $v_0, w_0, c_0 \in L^2(\Omega)$, $I^{app} \in L^2(\Omega\times(0,T))$, find $v \in W^{1,1}(0,T;H)$ $w \in L^2(0,T;[L^2(\Omega)]^N)$, and $c \in L^2(0,T;[L^2(\Omega)]^M)$ such that, $\forall t \in (0,T)$

$$\begin{cases} c_m\dfrac{\partial}{\partial t}(v(t),\phi) + a(v(t),\phi) + (I_{ion}(v(t),w(t),c(t)),\phi) = (I^{app},\phi) & \forall\phi\in H \\ \dfrac{\partial}{\partial t}(w(t),\psi) = (R(v(t),w(t)),\psi) & \forall\psi\in[L^2(\Omega)]^N \\ \dfrac{\partial}{\partial t}(c(t),\xi) = (S(v(t),w(t),c(t)),\xi) & \forall\xi\in[L^2(\Omega)]^M, \end{cases} \tag{4.1}$$

with suitable initial conditions on v, w, c, as given in (2.3). Here $(.,.)$ and $a(.,.)$ denote the inner product in $L^2(\Omega)$

$$(\eta,\chi) = \int_\Omega \eta\chi\,dx \qquad \forall\eta,\chi\in L^2(\Omega),$$

and the elliptic bilinear form

$$a(\lambda,\mu) = \int_\Omega (\nabla\lambda)^T D(\mathbf{x})\nabla\mu\,dx \qquad \forall\lambda,\mu\in H^1(\Omega),$$

respectively.
In a similar way, the variational formulation of the bidomain model can be written as follows.
Given $v_0, w_0, c_0 \in L^2(\Omega)$, $I^{app} \in L^2(\Omega\times(0,T))$, find $u_{i,e} \in W^{1,1}(0,T;H)$, $w \in L^2(0,T;[L^2(\Omega)]^N)$, and $c \in L^2(0,T;[L^2(\Omega)]^M)$ such that $\frac{\partial v}{\partial t} \in L^2(0,T;L^2(\Omega))$, $\frac{\partial w}{\partial t} \in L^2(0,T;[L^2(\Omega)]^N)$, $\frac{\partial c}{\partial t} \in L^2(0,T;[L^2(\Omega)]^M)$, and $\forall t \in (0,T)$

$$\begin{cases} c_m\dfrac{\partial}{\partial t}(v(t),\phi_i) + a_i(u_i(t),\phi_i) + (I_{ion}(v(t),w(t),c(t)),\phi_i) = 0 & \forall\phi_i\in H \\ -c_m\dfrac{\partial}{\partial t}(v(t),\phi_e) + a_e(u_e(t),\phi_e) - (I_{ion}(v(t),w(t),c(t)),\phi_e) = -(I_e^{app},\phi) & \forall\phi_e\in H \\ \dfrac{\partial}{\partial t}(w(t),\psi) = (R(v(t),w(t)),\psi) & \forall\psi\in[L^2(\Omega)]^N \\ \dfrac{\partial}{\partial t}(c(t),\xi) = (S(v(t),w(t),c(t)),\xi) & \forall\xi\in[L^2(\Omega)]^M \\ v(\mathbf{x},t) = u_i(\mathbf{x},t) - u_e(\mathbf{x},t), \end{cases} \tag{4.2}$$

with suitable initial conditions on v, w, c, as given in (2.1). Here $(.,.)$ denotes again the inner product in $L^2(\Omega)$, while $a_{i,e}(.,.)$ denote the elliptic bilinear forms

$$a_{i,e}(\lambda,\mu) = \int_\Omega (\nabla\lambda)^T D_{i,e}(\mathbf{x})\nabla\mu\, dx \qquad\qquad \forall\lambda,\mu\in H^1(\Omega),$$

respectively.
If, on the one hand, several theoretical results on reaction-diffusion equations can be applied to the monodomain model, on the other hand less is known on degenerate reaction-diffusion systems such as the bidomain model. We refer the reader to [6] for existence, uniqueness and regularity results, both at the continuous and the semi-discrete level, and to [24] for a convergence analysis of finite elements approximations. Both papers deals with the Fitz-Hugh-Nagumo (FHN) model of the gating system.
More results are known on the related eikonal approximation describing the propagation of excitation front (see for instance [2, 3, 11]), and a mathematical analysis of the bidomain model using Γ-convergence theory can be found in [1].

4.1 Semi-discrete formulation

Let $\mathcal{T}_h$ be a triangulation of $\Omega\subset\mathbb{R}^d$ $(d=2,3)$, namely $\Omega=\bigcup_{j=1}^N K_j$, where each $K_j = T_{K_j}(E)\in\mathcal{T}_h$, E is the reference element, a simplex (namely the triangle with vertices $(0,0)$, $(1,0)$, and $(0,1)$ when $d=2$ or the thetrahedron with vertices $(0,0,0)$, $(1,0,0)$, $(0,1,0)$, and $(0,0,1)$ when $d=3$) or the unit cube $[0,1]^d$ $(d=2,3)$, and where T_{K_j} is an invertible affine map. We define h as the maximum diameter of the elements of the triangulation. The associated finite element spaces X_h and Y_h (see e.g. [19] for an introduction to finite element methods) are defined as

$$X_h = \left\{\ \varphi_h\in C^0(\Omega)\,|\,\varphi_{h|K_j}\circ T_{K_j}\in\mathbb{P}_1(E)\right\}, \qquad Y_h = \left\{\ \varphi_h\in C^0(\Omega)\,|\,\varphi_{h|K_j}\circ T_{K_j}\in\mathbb{Q}_1(E)\right\},$$

where $\mathbb{P}_1(E)$ is the space of polynomials of degree at most one on E, whereas $\mathbb{Q}_1(E)$ is the space of polynomials of degree at most one with respect to each variable on E.
A semi-discrete problem in space is then obtained by applying a Galerkin procedure, using as finite dimensional space $V_h = X_h$ or $V_h = Y_h$, and choosing a basis for V_h. Let then $\{\varphi_i\}$ be the finite element basis, and let $M=(m_{kl})$, $A=(a_{kl})$ and $A_{i,e}=(a_{kl}^{i,e})$ be the symmetric mass and stiffnes matrices defined by

$$m_{kl} = \sum_{j=1}^N \int_{K_j} \varphi_k\varphi_l\, dx,$$

$$a_{kl} = \sum_{j=1}^N \int_{K_j} (\nabla\varphi_k)^T D(\mathbf{x})\nabla\varphi_l\, dx \qquad a_{kl}^{i,e} = \sum_{j=1}^N \int_{K_j} (\nabla\varphi_k)^T D_{i,e}(\mathbf{x})\nabla\varphi_l\, dx.$$

Numerical evaluation of such integrals is obtained by means of a 3rd order Gaussian rule. In the monodomain formulation, the finite elements approximation of the transmembrane potential $\boldsymbol{v}_h$ is the solution of

$$c_m M\frac{\partial \boldsymbol{v}_h}{\partial t} + A\boldsymbol{v}_h + M\, I_{ion}^h(\boldsymbol{v}_h,\boldsymbol{w}_h,\boldsymbol{c}_h) = MI_h^{app}. \tag{4.3}$$

On the other hand, the bidomain formulation for the finite element problem can be written in compact form as

$$\chi c_m\mathcal{M}\frac{\partial}{\partial t}\begin{pmatrix}\boldsymbol{u}_{i,h}\\ \boldsymbol{u}_{e,h}\end{pmatrix} + \mathcal{A}\begin{pmatrix}\boldsymbol{u}_{i,h}\\ \boldsymbol{u}_{e,h}\end{pmatrix} + \chi\begin{pmatrix} M\, I_{ion}^h(\boldsymbol{v}_h,\boldsymbol{w}_h,\boldsymbol{c}_h)\\ -M\, I_{ion}^h(\boldsymbol{v}_h,\boldsymbol{w}_h,\boldsymbol{c}_h)\end{pmatrix} = \begin{pmatrix}0\\ MI_{e,h}^{app}\end{pmatrix} \tag{4.4}$$

where the matrices $\mathcal{M}$ and $\mathcal{A}$ are given by

$$\mathcal{M} = \begin{pmatrix} M & -M\\ -M & M\end{pmatrix} \qquad\qquad \mathcal{A} = \begin{pmatrix} A_i & 0\\ 0 & A_e\end{pmatrix}. \tag{4.5}$$

Both equations (4.3) and (4.4) are coupled with the semidiscrete formulation of the dynamics of the gating and concentration variables

$$\frac{\partial \boldsymbol{w}_h}{\partial t} = R(\boldsymbol{v}_h,\boldsymbol{w}_h), \qquad \frac{\partial \boldsymbol{c}_h}{\partial t} = S(\boldsymbol{v}_h,\boldsymbol{w}_h,\boldsymbol{c}_h).$$

The bidomain formulation can be written alternatively in terms of $\boldsymbol{v}_h$ and $\boldsymbol{u}_{e,h}$ (or $\boldsymbol{v}_h$ and $\boldsymbol{u}_{i,h}$) by adding the two equations and substituting $\boldsymbol{u}_{i,h} = \boldsymbol{v}_h + \boldsymbol{u}_{e,h}$ in the first equation, obtaining

$$\begin{cases} c_m M \dfrac{\partial \boldsymbol{v}_h}{\partial t} + A_i \boldsymbol{v}_h + A_i \boldsymbol{u}_{e,h} + M\, I_{ion}^h(\boldsymbol{v}_h, \boldsymbol{w}_h, \boldsymbol{c}_h) = M\, I_{i,h}^{app} \\ \\ A_i \boldsymbol{v}_h + (A_e + A_i)\boldsymbol{u}_{e,h} = M(I_{i,h}^{app} - I_{e,h}^{app}). \end{cases} \tag{4.6}$$

Equation (4.6) above is a Differential-Algebraic Equation (DAE), that separates the differential variable $\boldsymbol{v}_h$ from the algebraic one $\boldsymbol{u}_{e,h}$. Such approach has been firstly used in [2] and [22], and sequently by many other authors.

4.2 Fully discrete approximation

In order to have a fully discrete approximation of the problem, we integrate in time systems (4.3) and (4.4) by means of a semi-implicit Euler scheme: the linear diffusion term is discretized implicitely, while the nonlinear reaction term (the ionic current I_{ion}) is treated explicitely. The mass matrix M is lumped to diagonal form by standard techniques. The ordinary differential system for the gating variables is integrated exactly after linearization around the potential at the previous time step.

The $j-$th gating variable at time step $n+1$ is given by

$$\boldsymbol{w}_j^{n+1} = \boldsymbol{w}_{j\infty}(\boldsymbol{v}_h^n) + (\boldsymbol{w}_j^n - \boldsymbol{w}_{j\infty}(\boldsymbol{v}_h^n)) \exp\left(-\frac{\Delta t}{\tau_{\boldsymbol{w}_j}(\boldsymbol{v}_h^n)}\right),$$

where

$$\boldsymbol{w}_{j\infty} = \alpha_j(\boldsymbol{v}^n)\tau_{\boldsymbol{w}_j}(\boldsymbol{v}^n) \qquad\qquad \tau_{\boldsymbol{w}_j}(\boldsymbol{v}^n) = \frac{1}{\alpha_j(\boldsymbol{v}^n) + \beta_j(\boldsymbol{v}^n)}$$

The system for the concentration variables is then integrated by a backward Euler scheme

$$\frac{\boldsymbol{c}_h^{n+1} - \boldsymbol{c}_h^n}{\Delta t} = S(\boldsymbol{v}_h^n, \boldsymbol{w}_h^{n+1}, \boldsymbol{c}_h^n).$$

This allows us to decouple the ODE system by solving with respect to the gating and concentration variables first, given the potential at the previous time step $\boldsymbol{v}_h^n$, and then solving, in the monodomain case, for $\boldsymbol{v}_h^{n+1}$

$$\chi c_m M \frac{\boldsymbol{v}_h^{n+1} - \boldsymbol{v}_h^n}{\Delta t} + A\boldsymbol{v}_h^{n+1} + \chi M I_{ion}^h(\boldsymbol{v}_h^n, \boldsymbol{w}_h^{n+1}, \boldsymbol{c}_h^{n+1}) = M I_h^{app}$$

and, in the bidomain case, for $\boldsymbol{u}_{i,h}^{n+1}$ and $\boldsymbol{u}_{e,h}^{n+1}$

$$\begin{cases} \chi c_m M \dfrac{\boldsymbol{v}_h^{n+1} - \boldsymbol{v}_h^n}{\Delta t} + A_i \boldsymbol{u}_{i,h}^{n+1} + \chi M I_{ion}^h(\boldsymbol{v}_h^n, \boldsymbol{w}_h^{n+1}, \boldsymbol{c}_h^{n+1}) = 0 \\ \\ -\chi c_m M \dfrac{\boldsymbol{v}_h^{n+1} - \boldsymbol{v}_h^n}{\Delta t} + A_e \boldsymbol{u}_{e,h}^{n+1} - \chi M I_{ion}^h(\boldsymbol{v}_h^n, \boldsymbol{w}_h^{n+1}, \boldsymbol{c}_h^{n+1}) = -M I_{e,h}^{app}, \end{cases}$$

where $\boldsymbol{v}_h^{n+1} = \boldsymbol{u}_{i,h}^{n+1} - \boldsymbol{u}_{e,h}^{n+1}$. With this choice (notice that one could solve for the potential first and update successively the gating and concentration variables), the semi-implicit method in the monodomain case requires to solve the linear system

$$\chi\left(\frac{c_m}{\Delta t} M + A\right)\boldsymbol{v}_h^{n+1} = \frac{c_m}{\Delta t} M \boldsymbol{v}_h^n - \chi M I_{ion}^h(\boldsymbol{v}_h^n, \boldsymbol{w}_h^{n+1}, \boldsymbol{c}_h^{n+1}) + M I_h^{app},$$

while, in the bidoman case, the associated linear system is

$$\left(\frac{\chi c_m}{\Delta t}\mathcal{M} + \mathcal{A}\right)\begin{pmatrix} \boldsymbol{u}_{i,h}^{n+1} \\ \boldsymbol{u}_{e,h}^{n+1} \end{pmatrix} = \frac{\chi c_m}{\Delta t}\mathcal{M}\begin{pmatrix} \boldsymbol{u}_{i,h}^{n} \\ \boldsymbol{u}_{e,h}^{n} \end{pmatrix} - \chi\begin{pmatrix} M I_{ion}^h(\boldsymbol{v}_h^n, \boldsymbol{w}_h^{n+1}, \boldsymbol{c}_h^{n+1}) \\ -M I_{ion}^h(\boldsymbol{v}_h^n, \boldsymbol{w}_h^{n+1}, \boldsymbol{c}_h^{n+1}) \end{pmatrix} + \begin{pmatrix} 0 \\ -M I_{e,h}^{app} \end{pmatrix},$$

where the matrices $\mathcal{M}$ and $\mathcal{A}$ are the ones defined in (4.5). The transmembrane potential $\boldsymbol{v}_h^{n+1}$ is uniquely determined, as in the continuous model, while $\boldsymbol{u}_{i,h}^{n+1}$ and $\boldsymbol{u}_{e,h}^{n+1}$ are determined up to the same additive time-dependent constant with respect to a reference potential. Such constant can be determined by imposing the

condition $\mathbf{1}^T M \boldsymbol{u}_{e,h}^{n+1} = 0$.
Notice that the semi-implict scheme above leads to a linear system with symmetric positive definite matrix in the monodomain case. On the other hand, in the bidomain case, the resulting linear system involves a symmetric positive semidefinite matrix, with a one dimensional kernel spanned by $(\mathbf{1}, \mathbf{1})^T$. These systems are solved by a preconditioned conjugate gradient algorithm (PCG), using as initial guess the solution at the previous time step.

General	$\chi = 10^3\ cm^{-1}$	$C_m = 10^{-3}\ mF/cm^2$
Monodomain	$\sigma_l = 1.2 \cdot 10^{-3}\ \Omega^{-1} cm^{-1}$	$\sigma_t = 2.5562 \cdot 10^{-4}\ \Omega^{-1} cm^{-1}$
Bidomain	$\sigma_l^e = 2 \cdot 10^{-3}\ \Omega^{-1} cm^{-1}$	$\sigma_t^e = 1.3514 \cdot 10^{-4}\ \Omega^{-1} cm^{-1}$
	$\sigma_l^i = 3 \cdot 10^{-3}\ \Omega^{-1} cm^{-1}$	$\sigma_t^i = 3.1525 \cdot 10^{-4}\ \Omega^{-1} cm^{-1}$
FHN model	$G = 1.5\ \Omega^{-1} cm^{-2}$	$\eta_1 = 4.4 \Omega^{-1} cm^{-1}$
	$v_{th} = 13\ mV$	$\eta_2 = 0.012$
	$v_p = 100\ mV$	$\eta_3 = 1$
CRN model	As in the original paper [7]	

Table 1: Parameter calibration for the numerical simulations

5 Numerical simulations

In this section we describe some numerical simulations. The computational domain is $\Omega = [0, 1] \times [0, 1]$, and the problem is discretized by $\mathbb{P}_1$ elements on an unstructured grid. We consider a two dimensional slab since the thickness of the atrial wall is far less significant than that of the ventricular one, and a two dimensional approximation is thus reasonable. We run monodomain and bidomain simulations, with both the modified FHN and the CRN cell model. In Table 1 we report the parameter calibration for the tests. The numerical simulations are run on MATLAB® 6.5.
In the first test we considered a vertex stimulation of the slab. We show the spread of excitation and the repolarization, in Figure 4 for the monodomain-FHN model, and, in Figure 5 for the monodomain-CRN model. For the latter model, the spike-and-dome profile of the Action Potential is more evident, as well as the longer time needed to recover the resting value of the potential, owing to the presence of the plateau phase, that is not captured by the simple FHN model.

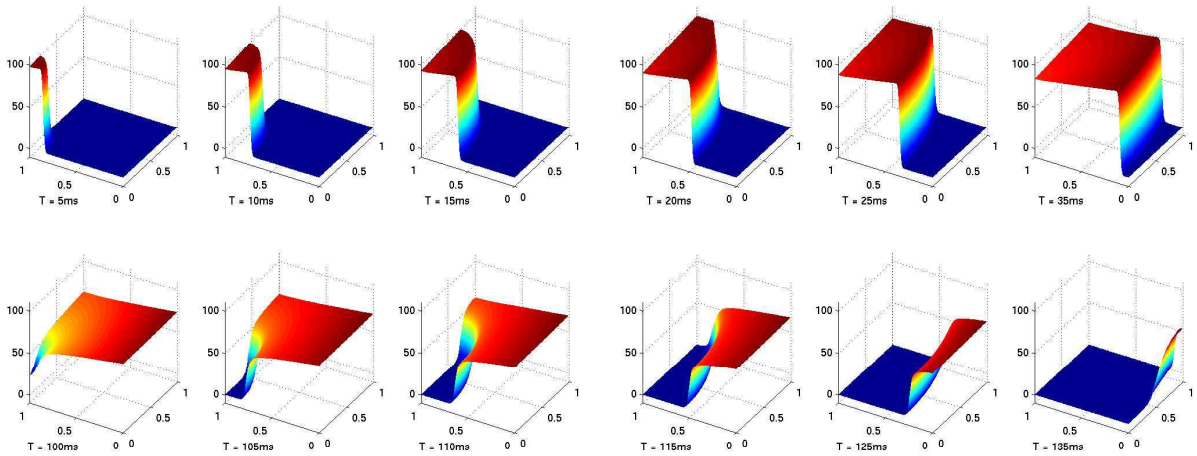

Figure 4: Monodomain FHN on a 2d slab: excitation and repolarization

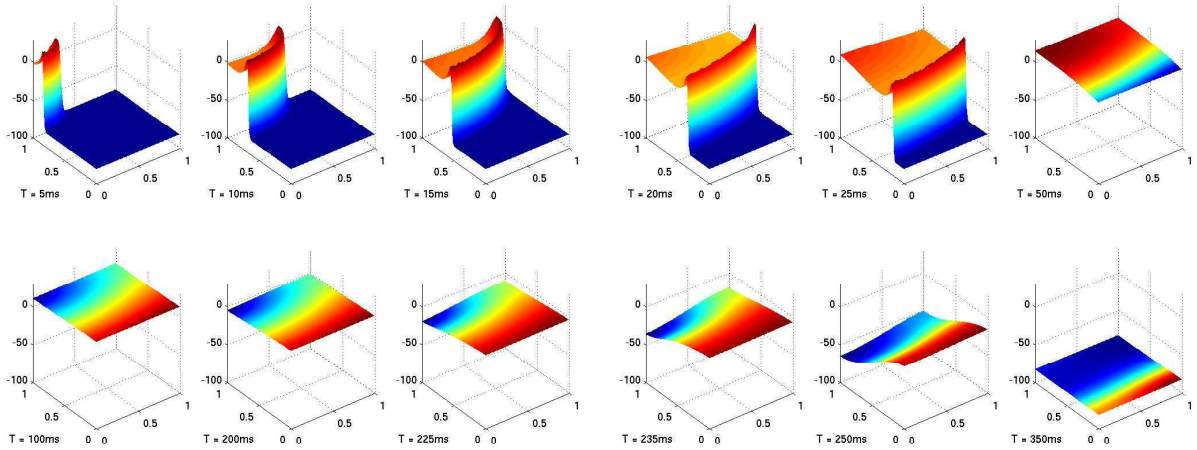

Figure 5: Monodomain CRN on a 2d slab: excitation and repolarization

In the second test we considered a central stimualtion of the slab. In Figure 6 we show the transmembrane potential v as well as the intracellular and extracellular potentials u_i and u_e, for the bidomain FHN model, at point (.2333,.5667) of the slab. In Figure 7 we show the spread of excitation and the action potential at point (.8,.7) for the bidomain CRN model.

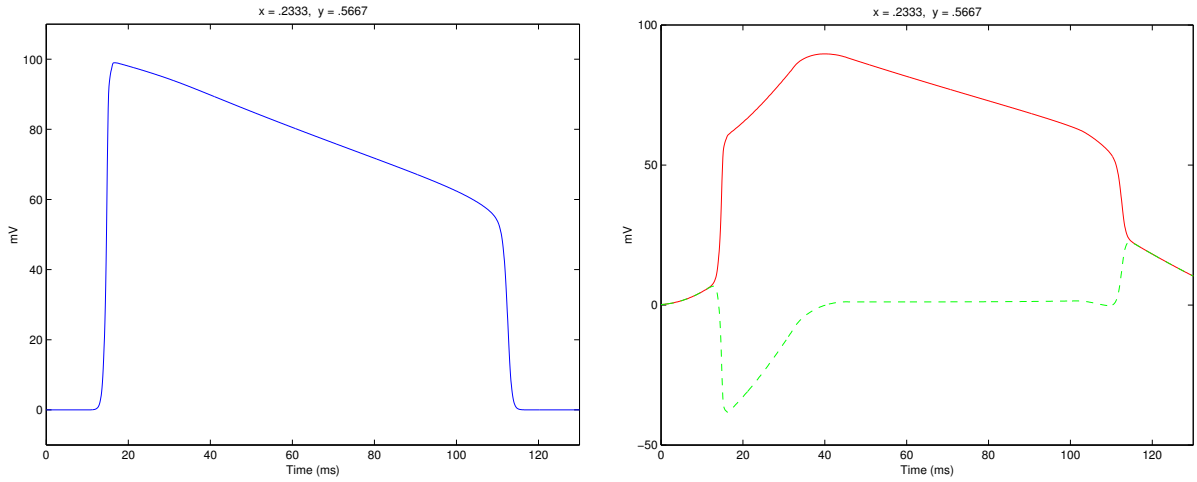

Figure 6: Bidomain FHN on a 2d slab: transmembrane potential v (left), intracellular u_i (solid line) and extracellular u_e (dotted line) potential at point (.2333,.5667)

In the third test, in order to simulate the presence of arteries or veins, we considered a two dimensional slab with a circular hole embedded. Since the vessel walls (both arterious and venous) are not excitable, we impose a non-conducting condition ($\boldsymbol{n} \cdot \nabla \boldsymbol{v} = 0$) on the border of the hole. We show the spread of excitation and the repolarization for the monodomain FHN model in Figure 8, and for the monodomain CRN in Figure 9. In Figure 10, a closer look allows to better appreciate the distorsion of the wavefront in the neighbourhood of the hole for both the FHN and CRN models.

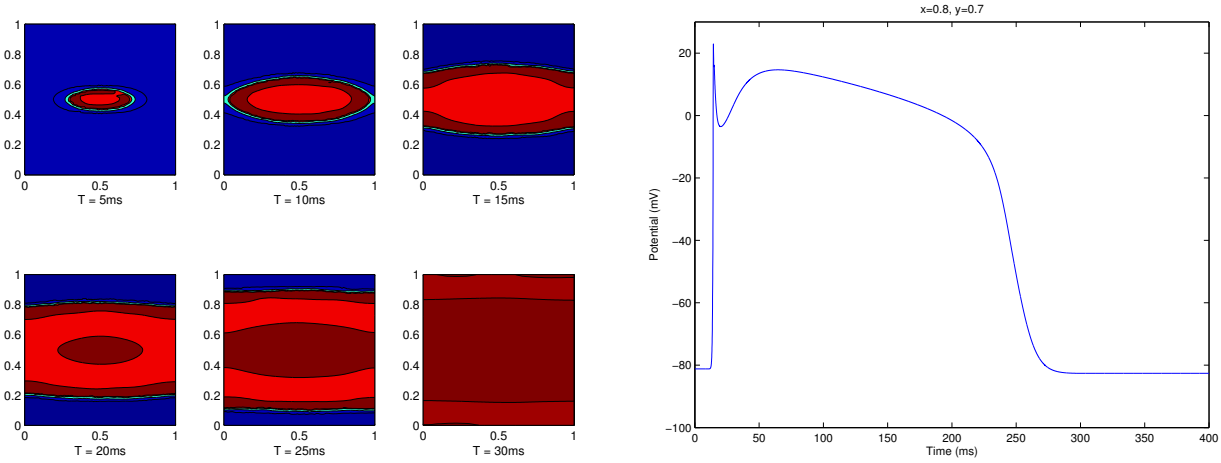

Figure 7: Bidomain CRN on a 2d slab: excitation spread (left) and transmembrane potential (right)

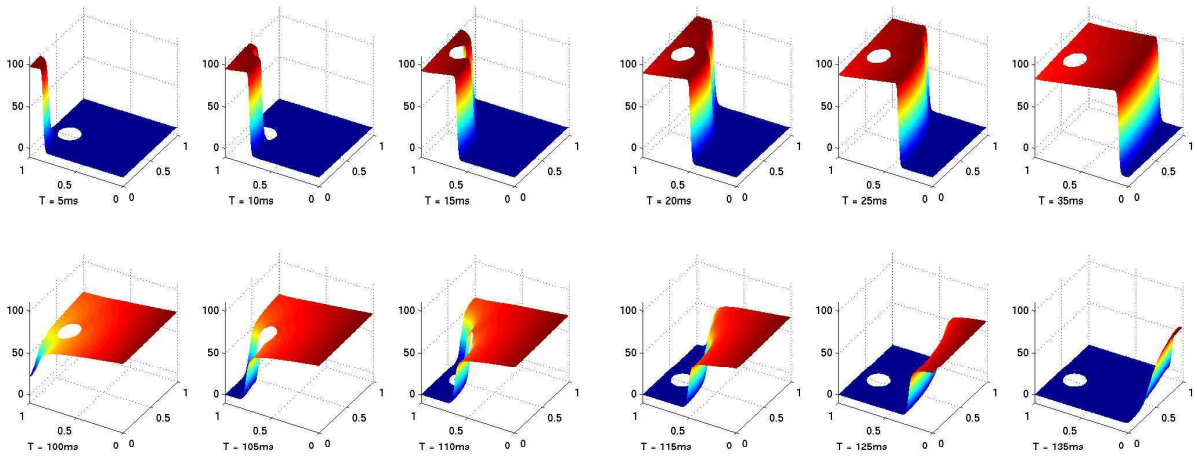

Figure 8: Monodomain FHN on a 2d slab with an hole: excitation and repolarization

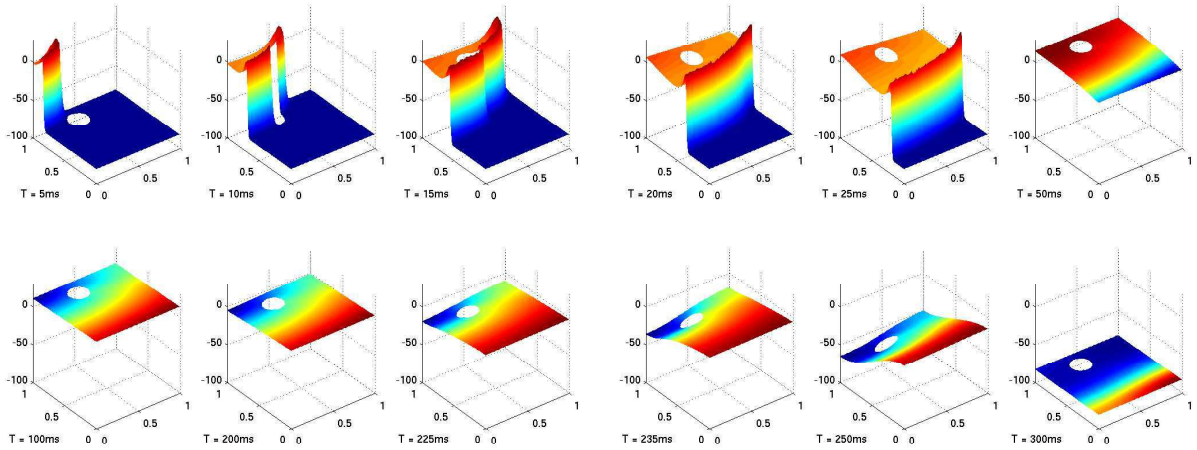

Figure 9: Monodomain CRN on a 2d slab with an hole: excitation and repolarization

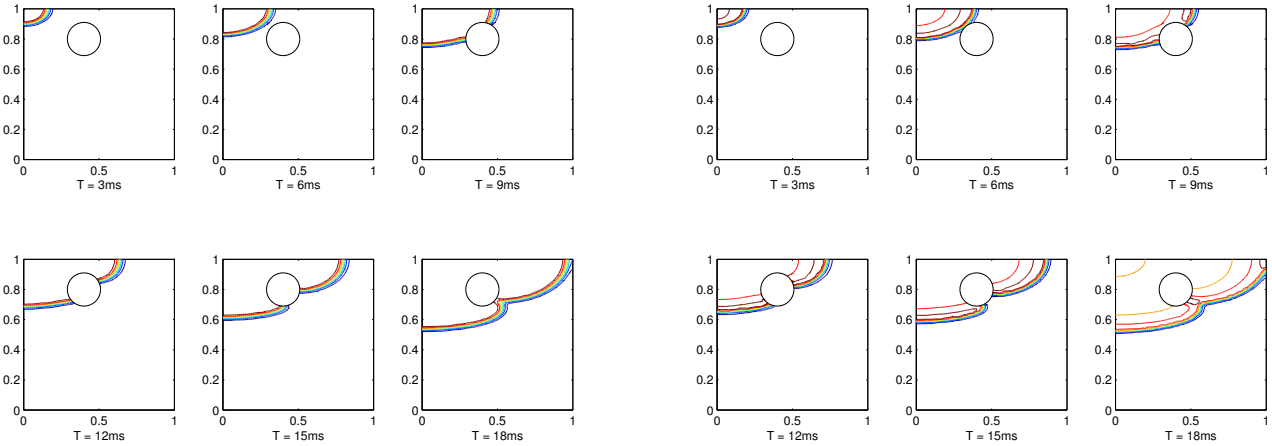

Figure 10: Propagation wavefront aroud an hole: monodomain FHN (left) and CRN (right) models

Finally, to analyze the cost of the two models, we compare their computational complexity in the first two test cases. The slab is discretized by an unstructured triangular grid consisting of 7744 nodes and 15166 elements. We report in Table 2 the CPU time needed to simulate complete a heartbeat (around 400msec) on a Dell Poweredge 4600 server. The higher level of accuracy in the description of the Action Potential provided by the CRN model requires a smaller step in the time integration. Moreover, at each time step with the CRN ionic model, one has to update 15 gating and 5 concentration variables on each point of the grid, whereas with the FHN ionic model only one gating variable has to be updated at each point of the grid. No adaptivity is introduced in the integration scheme for this comparison, and the fixed time steps are $\Delta t = 0.1$msec for the FHN models, and $\Delta t = 0.05$msec for the CRN models.

FHN		CRN	
Monodomain	Bidomain	Monodomain	Bidomain
3.1e+03	5.8e+03	5.6e+04	7.2e+04

Table 2: CPU time (in sec) for monodomain and bidomain models to simulate a complete heartbeat

6 Conclusions

We presented here an approach to simulate the propagation of the excitation fronts in the atrial cells, based on nonlinear models of reaction-diffusion type, considering both the monodomain and the bidomain approach. The ionic currents are expressed by the simple modified FHN model (in the Rogers-McCulloch variant), and by the more sophisticated CRN model, especially designed for human atrial cells. Numerical simulations on a two dimensional slab are given to show the behaviour of the excitation spread and the repolarization phase. Future work will focus on more general domains, on the simulation of spiral waves, and on the coupling of these models with models of pacemaker cells as the ones provided by O. Doessel and his collaborators (see for instance [25]).

References

[1] L. Ambrosio, P. Colli Franzone, and G. Savaré. On the asymptotic behaviour of anisotropic energies arising in the cardiac bidomain model. *Interfaces Free Bound.*, 2:213–266, 2000.

[2] P. Colli Franzone and L. Guerri. Spread of excitation in 3-D models of the anisotropic cardiac tissue, I: Validation of the eikonal approach. *Math. Biosci.*, 113:145–209, 1993.

[3] P. Colli Franzone, L. Guerri, M. Pennacchio, and B. Taccardi. Spread of excitation in 3-D models of the anisotropic cardiac tissue, II: Effect of the fiber architecture and ventricular geometry. *Math. Biosci.*, 147:131–171, 1998.

[4] P. Colli Franzone and L.F. Pavarino. A parallel solver for reaction-diffusion systems in computational electrocardiology. *Mathy. Mod. Meth. Appl. Sci.*, 14(6):883–911, 2004.

[5] P. Colli Franzone, L.F. Pavarino, and B. Taccardi. Simulating patterns of excitation, repolarization and action potential duration with cardiac Bidomain and Monodomain models. *Math. Biosci.*, 197(1):35–66, 2005.

[6] P. Colli Franzone and G. Savaré. Degenerate evolution systems modeling the cardiac electric field at micro and macroscopic level. In A. Lorenzi and B. Ruf, editors, *Evolution Equations, Semigroups and Functional Analysis*, pages 49–78. Birkhauser, 2002.

[7] M. Courtemanche, R.J. Ramirez, and S. Nattel. Ionic mechanisms underlying human atrial action potential properties: insights from a mathematical model. *Am. J. Physiol.*, 275 (Heart Circ. Physiol. 44):H301–H321, 1998.

[8] Y.E. Earm and D. Noble. A model of the single atrial cell: relation between calcium current and calcium release. *Pro. R. Soc. London B Biol. Sci.*, 240:83–96, 1990.

[9] C.S. Henriquez. Simulating the electrical behavior of cardiac tissue using the bidomain model. *Crit. Rev. Biomed. Engrg.*, 21:1–77, 1993.

[10] A.L. Hodgkin and A.F. Huxley. A quantitative description of membrane current and its application to conduction and excitation in nerve. *J. Physiol.*, 117:500–544, 1952.

[11] J.P. Keener. An eikonal-curvature equation for the action potential propagation in myocardium. *J. Math. Biol.*, 29:629–651, 1991.

[12] J.P. Keener and J. Sneyd. *Mathematical Physiology.* Springer-Verlag, 1998.

[13] J. Le Grice, B.H. Smaill, L.Z. Chai, S.G. Edgar, J.B. Gavin, and P.J. Hunter. Laminar structure of the heart: ventricular myocyte arrangement and connective tissue architecture in the dog. *Am. J. Physiol.*, 269 (Heart Circ. Physiol.):H571–H582, 1995.

[14] D.S. Lindblad, C.R. Murphey, J.W. Clark, and W.R. Giles. A model of the action potential and underlying membrane currents in a rabbit atrial cell. *Am. J. Physiol.*, 271:H1666–H1696, 1996.

[15] C. Luo and Y. Rudy. A dynamic model of the cardiac ventricular action potential. *Circ. Res.*, 74:1071–1096, 1994.

[16] A. Nygren, C. Fiset, L.Firek, J.W. Clark, D.S. Lindblad, R.B. Clark, and W.R. Giles. Mathematical model of an adult human atrial cell: the role of K+ currents in repolarization. *Circ. Res.*, 82:63–81, 1998.

[17] A.V. Panfilov. Spiral breakup as a model of ventricular fibrillation. *Chaos*, 8:57–64, 1998.

[18] A.V. Panfilov and A.V. Holden. *Computational biology of the heart*. Wiley, 1997.

[19] A. Quarteroni and A. Valli. *Numerical Approximation of Partial Differential Equations*. Springer-Verlag, Berlin, 1994.

[20] R.L. Rasmusson, J.W. Clark, W.R. Giles, E.F. Shibata, and D.L. Campbell. A mathematical model of a bullfrog cardiac pacemaker cell. *Am. J. Physiol.*, 259:H352–H369, 1990.

[21] J.M. Rogers and A.D. McCulloch. A collocation-galerkin finite element model of cardiac action potential propagation. *IEEE Trans. Biomed. Engnrg.*, 41:743–757, 1994.

[22] B.J. Roth. Action potential propagation in a thick strand of cardiac muscle. *Circ. Res.*, 68:162–173, 1991.

[23] B.J. Roth. How the anisotropy of the intracellular and extracellular conductivity influence stimulation of cardiac muscle. *J. Mat. Biol.*, 30:633–646, 1992.

[24] S. Sanfelici. Convergence of the galerkin approximation of a degenerate evolution problem in electrocardiology. *Numer. Meth. Part. Diff. Eq.*, 18(2):218–240, 2002.

[25] G. Seemann. *Modeling of Electrophysiology and tension development in the human heart*. PhD thesis, Universität Karlsruhe, 2005.

[26] D. Streeter. Gross morphology and fiber geometry in the heart. In R.M. Berne, editor, *Handbook of Physiology*, volume 1 (Sec. 2), pages 61–112. Williams and Wilnkins, 1979.

[27] R.L. Winslow, A. Varghese, D. Noble, C. Adlakha, and A. Hoythya. Generation and propagation of ectopic beats induced by spatially localized na-k pump inhibition in atrial network models. *Pro. R. Soc. London B Biol. Sci.*, 254:55–61, 1993.